scientific reports

Check for updates

OPEN

Optimization of emergency logistics for urban flooding with consideration of rainfall effects

Peiwen Zhang, Chenxing Zhang, Pan Zhang, Xuxian Yan✉ & Huawei Yang✉

Urban flooding frequently causes significant damage to infrastructure and facilities, leading to critical supply shortages in affected regions. Ensuring rapid and efficient distribution of relief supplies remains a key challenge during disaster response operations. This study proposes a two-stage optimization framework for emergency logistics. First, a supply distribution model is developed by integrating resource scarcity indices and disaster severity indices, optimized through a simulated annealing algorithm. Second, a vehicle routing model accounting for rainfall and dynamic vehicle speeds is established, solved using a hybrid Genetic Simulated Annealing algorithm to enhance computational efficiency. Ultimately, through simulation with randomly generated calculation examples, it was found that for the supply distribution model, the allocation model that takes into account both the resource scarcity index and the disaster index is more suitable for scenarios with an uneven distribution of disaster severity. The results of the model that takes into account the resource scarcity index, disaster index and waiting time index shows an improvement of 4% over the model that doesn't consider the resource scarcity index. The experimental results show that the proposed methodology not only adapts to varying disaster spatial patterns but also balances efficiency and equity under supply constraints, offering a scalable tool for designing resilient urban flood response systems.

Keywords Emergency logistics, Victim satisfaction, Urban flood, Vehicle routing optimization

In recent years, with the development of urbanization, the phenomenon of urban flooding has gradually increased[1]. According to Em-Dat, 164 floods occurred globally in 2023, affecting about 32.4 million people, resulting in 7,763 deaths and totaling $20.4 billion in damages[2]. The consequences of urban flooding disasters are manifold. In the aftermath of such disasters, the lack of clean water, food, shelter, and adequate medical care has a significant impact on affected populations[3]. Furthermore, the disruption of road networks can exacerbate the challenges faced in the wake of a disaster[4]. In light of the complex nature, uncertain outcomes, and extensive potential for damage associated with such disasters, it is imperative to exercise prudent stewardship of limited resources and to enhance the emergency management department's capacity to respond to crises in a timely and risk-mitigating manner[5]. It is thus crucial to examine the urban flood emergency logistics vehicles routing optimization, taking into account road accessibility, with the aim of guaranteeing the satisfaction of those involved in the disaster site.

This study employs a modeling and simulation methodology based on the concept of urban flooding emergency logistics processes, with the objective of enhancing the satisfaction of residents in affected areas and promoting innovation in modern urban flood emergency response.

The urban flooding emergency logistics processes can be described as follows: the emergency department proceeds to distribute the relief supplies from the Tier 1 distribution center to each secondary service center. Thereafter, the relief supplies from the Tier 2 service centers are distributed to each covered affected sites.

Figure 1 shows an example of a vehicle route in the context of disasters, where one vehicle transports supplies from a Tier 1 distribution center to two Tier 2 service centers, and then two vehicles transport supplies from two Tier 2 service centers to five different affected locations transport. Once the vehicle has serviced all affected locations, it will return to the Tier 2 service center from which it departed.

The structure of this article is as follows: In Sect. 2 surveys the existing literature on urban flood risk and the recent advancements in addressing the vehicle routing problem within the context of disasters. Section 3 presents the construction of the corresponding mathematical model. Section 4 details the design of an improved GA-SA algorithm. Section 5 demonstrates the simulation results of the applied models and algorithms. Finally, Sect. 6 provides a summary of the entire study.

School of Management Science and Engineering, Shanxi University of Finance and Economics, Taiyuan 030006, China. ✉email: yanxux@163.com; yanghuawei1990@163.com

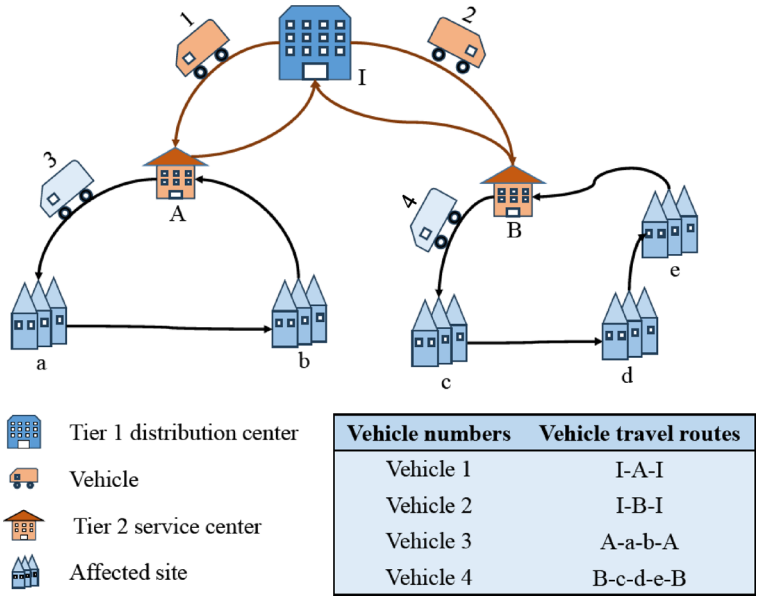

Vehicle numbers	Vehicle travel routes
Vehicle 1	I-A-I
Vehicle 2	I-B-I
Vehicle 3	A-a-b-A
Vehicle 4	B-c-d-e-B

Fig. 1. An example of a vehicle routing in the context of disasters.

No.	Authors	Focus	Limitations
1	Mitsakis et al.[6]	Rainfall impacts on traffic	Static speed assumptions
2	Pregnolato et al.[8]	The relationship of water depth and speed	No integration with routing optimization
3	Holguín-Veras et al.[11]	Deprivation cost minimization	Ignores psychological metrics
4	Zokaee et al.[17]	Two-stage optimization for earthquakes	Does not address flood-specific dynamics
5	Yang et al.[18]	Stochastic relief chains	Simplified victim satisfaction metrics

Table 1. The research gaps in existing studies.

Literature review

Urban flooding emergency logistics research has made notable progress in recent years, though challenges remain in addressing dynamic environmental changes and human-centered outcomes. Existing studies have primarily focused on quantifying transportation disruptions and optimizing logistical models, yet critical gaps persist in integrating real-time environmental dynamics and multi-dimensional human impacts.

In the realm of transportation disruption analysis, Mitsakis et al.[6] analyzed transportation metrics to quantify the impact of heavy rainfall on vehicular traffic, while Su et al.[7] developed an integrated simulation model for early warning of storm-induced traffic congestion. Pregnolato et al.[8] established a curve-fitted relationship between water depth and vehicle speed, and Suwanno et al.[1] evaluated evacuation times under different flood scenarios to identify alternative routes. Borowska-Stefańska et al.[9] further revealed that flooding-induced road closures, speed reductions, and detours significantly increase travel time, with spatial accessibility declines unaffected by inundation locations. These studies lay a foundation for understanding traffic dynamics but often rely on static or historical data, lacking real-time adaptability to evolving flood conditions—such as the exacerbated nighttime flooding severity noted by Shao et al.[10], which remains underexplored in predictive models.

In the field of emergency logistics modelling, Holguín-Veras et al.[11] pioneered the introduction of Deprivation Costs (DC) to quantify human suffering from service inaccessibility, inspiring subsequent studies such as Shi et al.[12] who developed a system dynamics model incorporating DC to analyse supply chain policies. Chen et al.[13] and Liu et al.[14] concentrated on the issue of medical supply routing in circumstances where demand was limited. In contrast, Khalili-Fard et al.[15] and Ghasemi et al.[16] advanced multi-stage, multi-objective models for logistics in the pre- and post-disaster context. As Zokaee et al.[17] and Yang et al.[18] have previously indicated, stakeholder satisfaction and time-sensitive allocation are of paramount importance. However, these models frequently fail to consider the dynamic interplay between flood progression and human behaviour. For instance, Valero et al.[19] discovered that vehicle mobility varies with flood debris dynamics, and Zang et al.[20] revealed that residential/commercial areas face disproportionate accessibility losses. Furthermore, human-centric factors such as evacuation psychology and equity in relief distribution have received insufficient attention, despite the focus of Okonta and Olaomi[21] on disaster response costs and the rescue route model developed by Zhu et al.[22] for minimising DC.

The focus and limitations of extant literatures are shown in Table 1. The majority of models fail to consider the dynamic coupling of rainfall intensity, road degradation, and logistics delays. The concept of victim satisfaction

is reduced to logistical metrics, with non-linear interactions between resource scarcity, disaster severity, and psychological distress being ignored. The allocation of supplies and the optimisation of routes are regarded as discrete stages, thereby impeding the development of comprehensive solutions when confronted with limitations in resources.

This study addresses the shortcomings of extant research and proposes the following innovations: The system incorporates dynamic vehicle speed models that are responsive to rainfall. A non-linear satisfaction function is proposed, incorporating elements of resource scarcity, disaster intensity, and waiting time. In the context of a two-stage optimization process, couples supply allocation is achieved through the implementation of adaptive routing. The proposed framework integrates environmental dynamics with human-centric metrics, thereby providing a scalable tool for resilient urban flood response.

Model

This article assumes that after a disaster, the decision-making department should respond quickly and decisively, downplay the control of logistics costs, and strive to increase the satisfaction of residents in the affected areas while reducing the sense of panic among the general public. Therefore, when distributing relief supplies after a disaster, considerations of minimizing costs or maximizing the effect-to-cost ratio should be ignored and instead the goal should be maximizing the rescue effect or maximizing overall satisfaction on the ground demand.

The problem examined can be described as follows: After a disaster, the initial distribution of relief supplies is carried out according to the needs of the affected locations and the extent of the disaster. The emergency department then distributes supplies from the Tier 1 distribution center to each secondary service center. The relief supplies will then be distributed from the Tier 2 service centers to all affected locations. Each service fleet first transports the relief supplies from the Tier 1 distribution center to the Tier 2 service centers, and then the Tier 2 service center carriers transport the relief supplies to the respective affected locations.

To facilitate the analysis, a series of assumptions were postulated for the purposes of the study:

- The number of Tier 1 distribution centers is known;
- The number of available Tier 2 service centers is known;
- Only one vehicle type is available for each Tier 1 distribution center;
- Only one vehicle type is available for each Tier 2 service center;
- The number of affected sites is known;
- The quantity of relief supplies stored at the Tier 1 distribution center is known, yet it is unable to simultaneously meet the total requirements at the affected sites;
- The maximum number of available vehicles is known and remains constant;
- Each affected sites can be served only once;
- Prior to the disaster, there were interconnecting roads between the service point and the demand point, and between the demand point and the demand point;
- As rainfall levels increase, vehicle speeds tend to decline;
- The level of rainfall is inversely proportional to the distance from the center point of the disaster, regardless of other factors;
- It is imperative that the vehicles return to the point of departure after completing all deliveries.

The problem solving process is detailed at Fig. 2.

The specific details regarding the model variable can be found in the Table 2.

The vehicle's actual speed model

The presence of water on the road surface, caused by rainfall, can result in vehicles skidding, particularly when travelling at high speeds. This can lead to a certain extent to a reduction in the speed at which vehicles are travelling, which also can affect the overall safety of the journey[23,24].

Given that the research background of this article is a flood disaster, the amount of rainfall is more than very heavy rainfall (very heavy rainfall are generally regarded as 140 mm/12 h). Consequently, the model has been amended to unify the units, then D'_{ij} is defined as Eq. 1, L_{ij} is defined as Eq. 2, and v'_{kij} in accordance with as Eq. 3.

$$D'_{ij} = \sqrt{\frac{D_{in}^2 + D_{jn}^2}{2} - \left(\frac{D_{ij}}{2}\right)^2} \tag{1}$$

$$L_{ij}\left(D'_{ij}\right) = \begin{cases} 0, & D'_{ij} > D_{Max} \\ \left(1 - \frac{D'_{ij}}{D_{Max}}\right) \times L_{Max}, & 0 \leq D'_{ij} \leq D_{Max} \end{cases} \tag{2}$$

$$v'_{kij} = v_k\left(1 - \left(0.03 \times ln\frac{L_{ij}}{48} + 0.07\right)\right) \tag{3}$$

The relief supplies requirement model

In the event of flooding, urban infrastructure and facilities are often compromised, leaving residents of affected areas in need of essential supplies and housing, include access to drinking water and food, as rainfall increases the damage to urban infrastructure and facilities increases and the supplies shortage increases[21].

In light of the relatively minor loss of supplies and facilities that occurs when the rainfall level is below heavy rainfall (heavy rainfall are generally regarded as 30 mm/12 h), this phenomenon is ignored in order to simplify

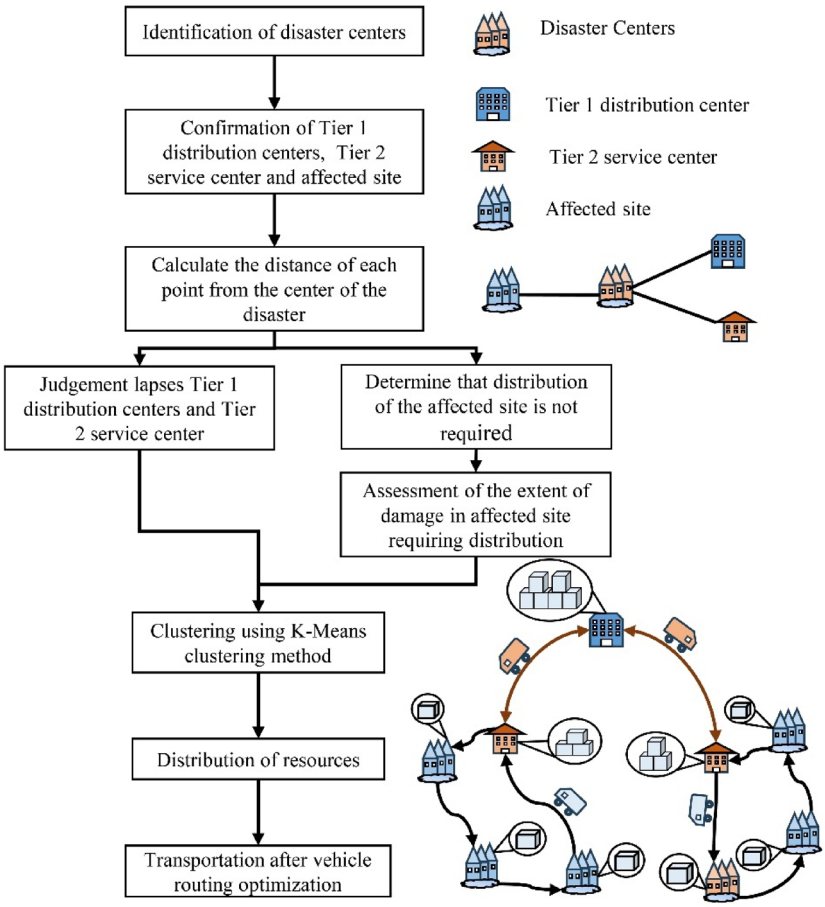

Fig. 2. Model scene flowchart.

the calculation of the model. Conversely, when the rainfall level is more than very heavy rainfall, the potential for transportation losses is significant, necessitating the inclusion of some redundancy of supplies. Thus the relationship between t δ_i, and L_i is defined as Eq. 4.

$$\delta_i = \begin{cases} 0, L_i \leq heavy\ rainfall \\ \frac{L_i - \text{heavy rainfall}}{\text{very heavy rainfall} - \text{heavy rainfall}}, \quad heavy\ rainfall < L_i \end{cases}, \quad \forall i \in \text{S, C} \tag{4}$$

Therefore, C_e^i is defined as in Eq. 5.

$$C_e^i = \delta_i \cdot p_i \cdot \lambda, \forall i \in \text{C} \tag{5}$$

The calculation of δ_i will vary depending on the nature of the hazard. For instance, in the case of seismic events, δ_i is determined by the magnitude of the event and the distance from the epicenter.

The satisfaction model

The panic index of the residents by those affected by a disaster is directly proportional to the severity of the disaster, the extent of supply shortages, and the duration of the wait for assistance. In situations where the disaster is more severe, there is a greater degree of relief supplies shortage, and rescue is delayed for a longer period of time, the psychological distress experienced by victims increases exponentially.

The relationship between C_v^i, C_e^i, and C_i, is shown in Eq. 6.

$$C_v^i = \frac{C_e^i - C_i}{C_e^i}, \forall i \in \text{C} \tag{6}$$

The relationship between L_r^i, L_i and L_{Max}, is shown in Eq. 7.

$$L_r^i = \frac{L_i}{L_{Max}}, \forall i \in \text{C} \tag{7}$$

t_i is defined as in Eq. 8.

Variables	Description	Unit
S	The set of service points	
C	The set of demand points	
N	The set of carriers	
m	The number of affected sites to be distributed	
Q_k	The maximum load capacity of vehicle k	tons
D_{ij}	The distance between arc i, j	km
L_i	The amount of rainfall at point i	mm/12 h
D'_{ij}	The distance of arcs i, j from the distribution center	km
L_{ij}	The amount of rainfall in arc i, j	mm/12 h
v_k	The theoretical speed of vehicle k	km/h
v'_{kij}	The actual speed of vehicle k on arc i, j	km/h
C_e^i	The relief supplies requirement	
p_i	The size of the population	persons
λ	The relief supplies requirement per unit of person	tons
C_v^i	The relief supplies shortages index at point i	
C_i	The distribution of relief supplies at point i	
L_r^i	The damage index at point i	mm/12 h
L_i	The amount of rainfall at point i	mm/12 h
L_{Max}	The maximum rainfall among the affected sites	mm/12 h
t'_i	The theoretical time spent from the Tier 1 distribution center to point i	hours
t_r^i	The waiting time index at point i	hours
t_i	The waiting time at point i	hours
M_i	The satisfaction of residents at point i	
μ	The maximum supply shortage ratio	
Q_{Max}	The supply storage capacity of the Tier 1 distribution center	tons
$\bar{M}$	The average satisfaction of the residents of the distributed affected sites	

Table 2. Model variable list.

$$t_j = \sum_{i \in (C \cup S)} \sum_{k \in N} (t_i + t_s^i + \frac{D_{ij}}{v'_k}) \cdot X_{ij}^k, \forall j \in C, i \neq j \tag{8}$$

t'_i, is defined by Eq. 9.

$$t'_i = \frac{D_{0i}}{v_k} \cdot X_{0i}^k \tag{9}$$

The relationship between t_r^i, t_i and t'_i, is shown in Eq. 10.

$$t_r^i = \frac{t_i}{t'_i}, \forall i \in C \tag{10}$$

The deprivation cost on the affected groups is rising exponentially[25]. The level of satisfaction among residents of the disaster site is inversely correlated with the panic index among those same residents. In other words, as a result of the more widespread distribution of supplies, a reduction in rainfall, and a decrease in waiting times, the decline in the panic index is accompanied by an increase in satisfaction among residents of the disaster site, therefore M_i satisfies Eq. 11.

$$M_i = \frac{1}{e^{C_v^j \cdot L_r^i \cdot t_r^i}} \cdot 100\%, \forall i \in C \tag{11}$$

The distribution models

Distribution model I

This distribution model only considers the resource shortage index.

According to Eq. 11, when C_v^i is smaller, M_i is larger. So the distribution model I aims at $\sum C_v^i$ minimization as Eq. 12.

$$min \sum_{i \in C} C_v^i = \sum_{i \in C} \frac{c_e^i - C_i}{c_e^i} \tag{12}$$

Finally, based on the assumption, the distribution of resources should be lower than the maximum supply shortage ratio, and each transport vehicle must not be overloaded. Thus, the constraint functions are defined as Eqs. 13–14.

$$0 < C_v^i \leq \mu, \forall i \in C \tag{13}$$

$$\sum_{i \in C} C_i \leq Q_{Max} \tag{14}$$

Distribution model II

This distribution model considers the resource shortage index and damage index.

According to Eq. 11, when C_v^i and L_r^i is smaller, M_i is larger. So the distribution model I aims at $\sum C_v^i \cdot L_r^i$ minimization as Eq. 15.

$$min \sum_{i \in C} C_v^i \cdot L_r^i = \sum_{i \in C} \frac{c_e^i - C_i}{c_e^i} \cdot \frac{L_i}{L_{Max}} \tag{15}$$

Constraint functions are the same as Eqs. 13–14.

The vehicle routing optimization model

Taking $\bar{M}$ as the model optimization objective, the objective function is Eq. 16.

$$max \bar{M} = \sum_{i \in C} M_i/m = \sum_{i \in C} \frac{1}{e^{C_v^j \cdot L_r^i \cdot t_r^i}} \cdot 100\%/m \tag{16}$$

Then build the constraint functions as defined in Eqs. 17–22.

$$\sum_{k \in N} X_{ij}^k = 1, \forall i, j \in (C \cup S) \tag{17}$$

$$\sum_{j \in (C \cup S)} X_{ij}^k = y_i^k, k \in N, i \in (C \cup S), i \neq j \tag{18}$$

$$\sum_{j \in (C \cup S)} X_{ij}^k = y_j^k, k \in N, j \in (C \cup S), i \neq j \tag{19}$$

$$\sum_{j \in (C \cup S)} c_i \cdot y_i^k \leq Q_k, k \in N \tag{20}$$

$$\sum_{j \in C} X_{ij}^k = \sum_{j \in C} X_{ji}^k, k \in N, i \in S \tag{21}$$

$$\sum_{i \in S} \sum_{j \in S} X_{ij}^k = 0, k \in N, i \neq j \tag{22}$$

where Eqs. 17–19 indicate that each demand point is served by only one carrier. Equation 20 indicates that the quantity of demanded supplies at the demand point is not greater than the maximum load capacity of the vehicle. Equation 21 indicates that the vehicle has to return to the departure point after departing from the service point. And Eq. 22 indicates that the vehicle is not allowed to travel from the service point to another service point.

Finally, define the decision variable functions are Eqs. 23–24.

$$X_{ij}^k = \begin{cases} 0, \ vehicle\ k\ don't\ travel\ on\ arc\ (i,j) \\ 1\ vehicle\ k\ travel\ on\ arc\ (i,j) \end{cases} \tag{23}$$

$$y_i^k = \begin{cases} 0, \ vehicle\ k\ don't\ distribute\ i\ point \\ 1, vehicle\ k\ distribute\ i\ point \end{cases} \tag{24}$$

Algorithm

The vehicle routing problem with multiple vehicles in multiple car parks belongs to NP-hard problem[26]. The emergency route optimization model constructed in this article is a nonlinear planning model. As the quantity of data increases, the computational volume grows exponentially, and exhaustive enumeration is no longer a viable method for finding an exact solution. Therefore, heuristic intelligent optimization algorithms must be employed

GA-SA Process	
Input:	Population size M, mutation probability α_1, crossover probability α_2, annealing speed α, evaluation function F.
Output:	X_{best}
Set1:	K-Means clustering
Set2:	generating the initial solution set {X}
Set3:	global optimum $X_{best}=X_0$, current optimal solution $X_{best1}=X_0$
Set4:	**while** the number of iterations is not greater than the number of terminations
	while temperature not lower than the termination temperature
	use roulette to select a solution X
	with α_1 probability of mutation to generate X_{new}
	with α_2 probability of crossover to generate X_{new}
	if $F(X_{new}) > F(X_{best1})$ then
	if $F(X_{new}) > F(X_{best})$ then
	$X_{best} = X_{new}$
	else $X_{best1} = X_{new}$
	end if
	else
	if meets simulated annealing acceptance criteria then
	$X_{best1} = X_{new}$
	end if
	end if
	updated simulated annealing temperatures and roulette parameters
	end while initialize temperature
	end while
Set5:	output X_{best}

Table 3. Detailed pseudo-code for the GA-SA algorithm.

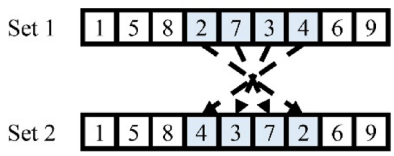

Fig. 3. Inverted mutation operator.

to address the problem. A comprehensive review of the literature reveals that the majority of scholars employ genetic algorithm (GA) to address such problems. However, GA is prone to yielding local optimal solutions and are not well-suited for addressing large-scale computational problems. Accordingly, this article employs a Simulated Annealing Algorithm (SA) for resource allocation and a Genetic Simulated Annealing Algorithm (GA-SA) for route optimization model resolution[27]. This approach mitigates the proclivity of the algorithm to converge prematurely on a local optimal solution. The GA-SA process is shown in Table 3.

Mutation to generate new solution

The mutation operator was performed using an inverted mutation, in which two positions in the chromosome were randomly selected, the interval of elements to be changed in order was determined, and the order of elements within the mutated interval was arranged in reverse order. As in Fig. 3, the first step selects the blue interval [2,7,3,4] as the mutation interval and the second step arranges the elements within the blue interval in reverse order.

Crossover to generate new solution

Crossover operations use the sequential crossover, randomly selects two positions in the chromosome, determines the interval of elements to be crossed, swaps the selected intervals in the two existing solutions, removes the elements in the original solution that are duplicates of the swapped intervals, and places the swapped ones Intervals outside of the exchanged intervals in the order. As shown in Fig. 4, the first step selects the blue interval [2,7,3] and [1,4,6] as the mutation interval, in the second step, the elements in the blue intervals of the two solutions are swapped and marked away the duplicate elements in gray and places the elements of the swapped intervals in the free position in the order.

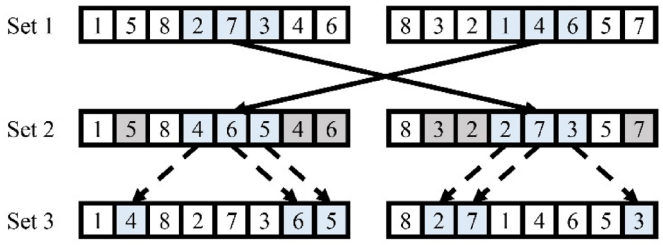

Fig. 4. Sequential crossover operator.

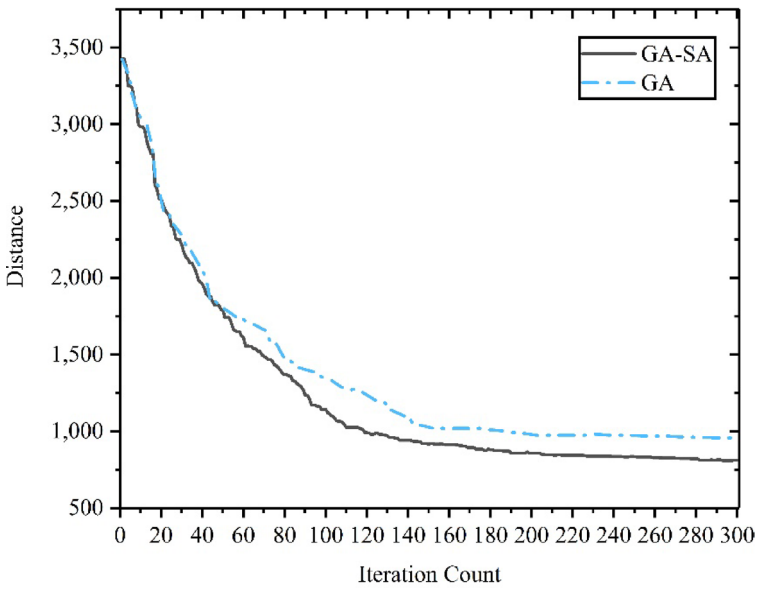

Fig. 5. Iterative comparison chart of two algorithms.

Algorithm performance comparison

The GA-SA algorithm is tested for large-scale computations using Solomons' C101 dataset. Compared with the GA, the solution time of GA-SA increases by 29 s and the distance of the calculated results decreases by 145.08. It can be seen from Fig. 5 that the convergence speed of GA-SA algorithm is close to that of GA, but the quality of the solution is higher, so GA-SA algorithm is better than GA in solving large sets - scaled data sets.

GA have been demonstrated to encounter challenges in addressing complex constraints, and a solitary genetic algorithm encoding is inadequate in providing a comprehensive representation of the constraints inherent in an optimization problem. Consequently, the computational time required to consider these constraints invariably increases. The simulated annealing component of GA-SA has been demonstrated to effectively address these constraints by employing state transfer probabilities and acceptance criteria that are suitably designed. This enhanced functionality facilitates the optimization of operational efficiency, thereby enhancing the algorithm's ability to address a comprehensive array of practical constraints. Consequently, this enhanced functionality results in the generation of an emergency logistics program for urban flooding that exhibits a greater degree of alignment with the actual circumstances of the situation.

Simulation analysis

In the example, there are 1 Tier 1 distribution center, 10 Tier 2 service centers, and 20 affected sites in the affected area, and the location coordinates of each point are mapped on the plane coordinates of 120 km × 120 km, and the actual distance between each node is expressed by the Euclidean distance on the plane coordinates, in which the point 0 is the Tier 1 distribution service center, the points I-X are the Tier 2 service centers, the points 11–29 are the ripple effect affected sites, and the point 30 is the disaster center point. points, and point 30 is the center of the disaster.

The total amount of supplies stored in the Tier 1 distribution center is 300 tons, and the number of carriers can be distributed to all Tier 2 service centers at the same time; the number of vehicles is 10; the theoretical speed of the vehicles is 80 km/h; the transport capacity of the vehicles is 60 tons; and the service time for each point of demand is 0.5 h. Specific data are shown in Tables 4 and 5.

According to the coordinates of the location of each point, the rainfall of each point is calculated according to Eq. 1, and according to the results, it shows that the rainfall of the secondary service center points of V, VI,

No.	Location (X, Y)/km	No.	Location (X, Y)/km	No.	Location (X, Y)/km
0	(10,116)	IV	(60,40)	VIII	(70,71)
I	(20,25)	V	(83,89)	IX	(92,102)
II	(29,45)	VI	(55,65)	X	(60,60)
III	(41,43)	VII	(55,75)		

Table 4. Service points data.

No.	Location (X, Y)/km	p_i/Persons	No.	Location (X, Y)/km	p_i/Persons
11	(10,22)	$0.33 \cdot 10^4$	21	(32,81)	$0.43 \cdot 10^4$
12	(25,21)	$0.52 \cdot 10^4$	22	(33,91)	$0.31 \cdot 10^4$
13	(26,13)	$0.28 \cdot 10^4$	23	(75,91)	$0.13 \cdot 10^4$
14	(16,50)	$0.21 \cdot 10^4$	24	(62,74)	$0.21 \cdot 10^4$
15	(40,67)	$0.32 \cdot 10^4$	25	(70,67)	$0.23 \cdot 10^4$
16	(36,53)	$0.23 \cdot 10^4$	26	(70,53)	$0.25 \cdot 10^4$
17	(42,61)	$0.22 \cdot 10^4$	27	(73,60)	$0.31 \cdot 10^4$
18	(53,72)	$0.13 \cdot 10^4$	28	(90,67)	$0.25 \cdot 10^4$
19	(113,67)	$0.36 \cdot 10^4$	29	(80,75)	$0.22 \cdot 10^4$
20	(43,39)	$0.24 \cdot 10^4$	30	(65,75)	$0.26 \cdot 10^4$

Table 5. Disaster points data.

No.	D'_{ij}/km	L_i/mm/12 h	C_e^i/t	No.	D'_{ij}/km	L_i/mm/12 h	C_e^i/t
0	68.6	0	- [1]	16	36.4	108	16.4
I	67.3	4.4	-	17	26.9	139.8	22.1
II	46.9	72.8	76.7	18	12.4	188.4	18.9
III	40.0	95.9	86.8	19	48.7	66.7	12.1
IV	35.4	111.3	131.4	20	42.2	88.5	12.9
V	22.8	153.6	-	21	33.5	117.7	34.6
VI	14.1	182.7	-	22	35.8	110	22.7
VII	10.0	196.5	-	23	18.9	166.6	16.3
VIII	6.4	208.5	-	24	3.2	219.3	36.4
IX	38.2	101.9	132.2	25	9.4	198.5	35.5
X	15.8	177	-	26	44.3	81.5	11.8
11	76.4	0	0	27	9.4	198.5	47.9
12	67.2	4.7	0	28	26.2	142.2	25.7
13	73.2	0	0	29	15.0	179.7	30.2
14	55.0	45.6	3	30	0.0	230	47.7
15	26.2	142.2	32.9				

Table 6. Results of arithmetic operations. [1]“ - ” denotes that supplies are not required for Tier 1 distribution center and inactive Tier 2 service centers.

VII, VIII, and X is more than 140 mm/12 h, and they have been subjected to extraordinarily heavy rainfall, and it is considered that their supplies and facilities have been damaged, so it is not possible to activate these five Tier 2 service centers. Meanwhile, the rainfall of affected sites 11, 12, and 13 is less than 30 mm/12 h, and it is considered that they are basically not affected by the disaster, so the distribution of these three affected sites is not considered in the first distribution after the disaster. The specific arithmetic results are shown in Table 6.

Using the K-Means clustering algorithm, the remaining affected sites are clustered with the open Tier 2 service centers, and the clustering results are obtained as follows: there are no service points in the Tier 2 service center I; the set of assigned affected sites of the Tier 2 service center II is (14, 16, 21, 22); the set of assigned affected sites of the Tier 2 service center III is (15, 17, 18, 20); the Tier 2 service center IV is assigned a collection of affected sites as (24, 25, 26, 27, 30); and the Tier 2 service center IX is assigned a collection of affected sites as (19, 23, 28, 29). According to Eqs. 4–5, the supplies demand of each demand point is calculated, and the supplies demand of the Tier 2 service centers is calculated based on the clustering results. Due to the limited material reserve of the Tier 1 distribution center, which is only 300 t, the total supplies demand of all affected sites is

427.1 t, which can not be distributed to meet the supplies of all affected sites at one time, and the total amount of distributed supplies is 70.24% of the total amount of required supplies. Therefore, it is necessary to distribute the supplies to the affected sites, and the distribution is based on the Distribution Model I and Distribution Model II.

In this study, the allocation of supplies at each demand point is done by SA with the parameters of temperature = 1000; alpha = 0.99; the minimum resource satisfaction rate is 30%; the number of iterations is 300; and the number of times the program is run is 10 times by using Python 3.6 software. According to the Distribution Model I, the result is: $\min \sum_{j \in C} C_v^j = 4.59$, the total amount of distributed supplies is 300 t. According to the Distribution Model II, the result is: $\min \sum_{j \in C} C_v^j \cdot L_r^i = 2.82$, the total amount of distributed supplies is 300 t. The specific distribution results are shown in Table 7.

After the distribution, the problem is solved using the GA-SA with the following parameters: number of populations = 30; mutation probability = 50%; crossover probability = 30%; inversion probability = 20%; annealing temperature = 1000; annealing coefficient = 0.99; iteration number 300 times; number of program runs 10 times.

According to the results of distribution model I, the solution is obtained as: $\max -M = 69.82\%$; the optimal routes are [0, 2, 16, 21, 22, 14, 2], [0, 3, 20, 15, 17, 18, 3], [0, 4, 24, 30, 4, 25, 26, 4], [0, 9, 23, 28, 9, 29, 19, 9, 27, 9]; the generated optimal route diagram is shown in Fig. 6.

According to the results of distribution model II, the solution is obtained as: $\max -M = 70.00\%$; the optimal routes are [0, 2, 21, 22, 14, 16, 2], [0, 3, 20, 17, 15, 18, 3], [0, 4, 25, 4, 30, 26, 4, 24, 4], [0, 9, 27, 23, 9, 29, 28, 9, 19, 9]; the generated optimal route diagram is shown in Fig. 7.

Distribution model validity analysis

Analysis of results

Observing the allocation results of allocation model I, it is found that the resource scarcity index of the affected sites with small resource demand is relatively lower, and it is more inclined to prioritize the affected sites with lower demand; while observing the allocation results of allocation model II, it is found that the resource scarcity index of the affected sites with larger rainfall is relatively lower, and it is more inclined to prioritize the affected sites with larger rainfall.

Analysis of application scenario

Distributional model I is more appropriate in the scenario of a more balanced disaster, in which the distributional model maximizes the marginal utility of the supplies.

Distribution model II is more suitable for unevenly affected areas, in which the distribution model gives higher priority to the more affected areas.

Shortcoming

Observing the distribution results of the two distribution models, there is a situation that individual affected sites with low resource scarcity are not prioritized in distribution model I; distribution model II does not appear to make the resource scarcity index of the disaster-affected centers the lowest among all affected sites, and individual affected sites with large rainfall are not prioritized. It indicates that the algorithms for running the two distribution models are not properly selected, the local optimal solution appears, the global optimal solution is not obtained, and there is still room for further optimization of the algorithms in the distribution stage.

No.	C_i/t		No.	C_i/t	
	Model I	Model II		Model I	Model II
I	- [1]	-	16	6.18	15.98
II	54.01	52.49	17	18.14	16.47
III	59.05	44.67	18	18.12	13.24
IV	73.88	124.73	19	11.71	8.54
V	-	-	20	7.89	4.17
VI	-	-	21	27.89	20.44
VII	-	-	22	17.07	13.59
VIII	-	-	23	11.82	14.87
IX	113.06	78.11	24	25.47	29.03
X	-	-	25	15.69	32.14
11	0	0	26	8.37	10.84
12	0	0	27	39.21	17.5
13	0	0	28	23.21	25.26
14	2.87	2.48	29	27.11	29.44
15	14.9	10.79	30	24.35	35.22

Table 7. Results of the distribution of resources. [1]" - " denotes that supplies are not required for Tier 1 distribution center and inactive Tier 2 service centers.

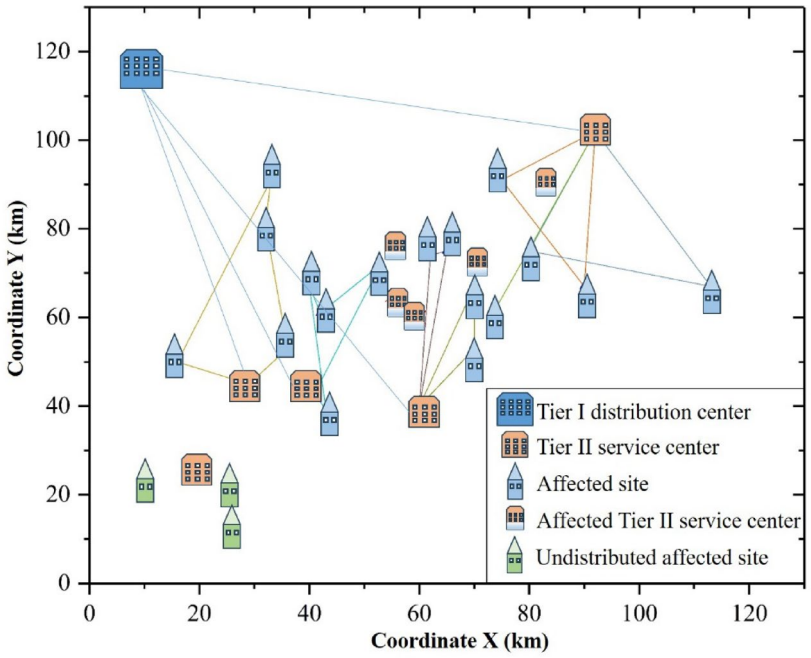

Fig. 6. Distribution mode l optimal route.

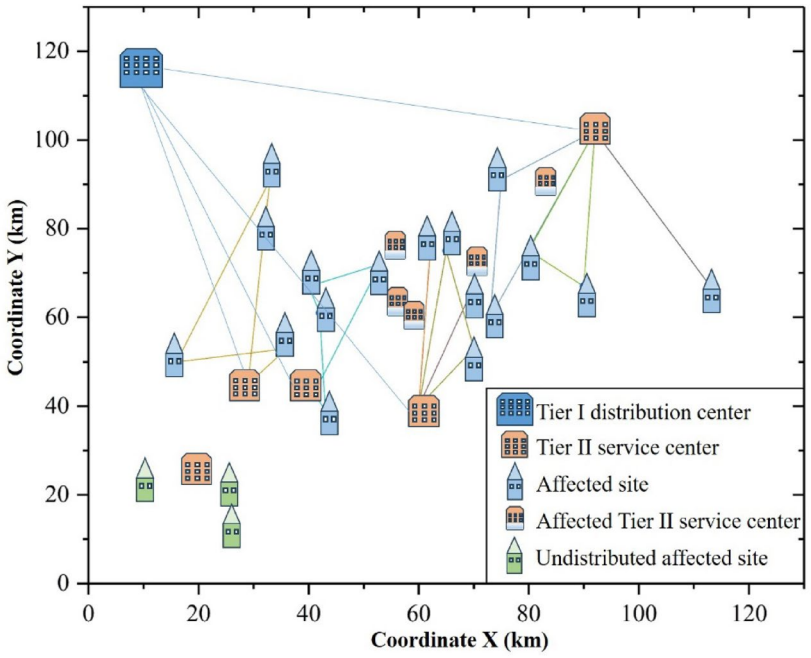

Fig. 7. Distribution model II optimal route.

Route optimization model validity analysis

Using the distribution results of distribution model II, the optimal route is derived from the route optimization model that considers only the damage index and the waiting time index: [0, II, 16, 14, 22, 21, II], [0, III, 20, 18, 15, III, 17, III], [0, IV, 30, IV, 25, 24, IV, 26, IV], [0, IX, 27, 29, 23, IX, 28, 19, IX], the solution is obtained as: $\max -M = 67.18\%$.

The optimal route is derived from the route optimization model that considers only the total distribution time: [0, II, 16, 21, 22, 14, II], [0, III, 20, 17, 15, III, 18, III], [0, IV, 25, IV, 30, 24, IV, 26, IV], [0, IX, 23, 27, 29, IX, 28, 19, IX], the solution is obtained as: $\max -M = 67.94\%$.

The results of route optimization models are presented in Table 8.

Tier II service centers Number	Original route optimization model	Don't consider the resource scarcity index	Consider only the total distribution time
II	II-21-22-14-16-II	II-16-14-22-21-II	II-16-21-22-14-II
III	III-20-17-15-18-III	III-20-18-15-III III-17-III	III-20-17-15-III II -18-III
IV	IV-25-IV IV-30-26-IV IV-24-IV	IV-30-IV IV-25-24-IV IV-26-IV	IV-25-IV IV-30-24-IV IV-26-IV
IX	IX-27-23-IX IX-29-28-IX IX-19-IX	IX-27-29-23-IX IX-28-19-IX	IX-23-27-29-IX IX-28-19-IX

Table 8. Vehicle routing optimization results.

	Average satisfaction $\bar{M}$	Percentage decline (%)
Original route optimization model	70.00%	/
Don't consider the resource scarcity index	67.18%	4.03
Consider only the total time	67.94%	2.94

Table 9. Comparative analysis results of vehicle routing optimization models.

v_k(km/h)	$\bar{M}_1$	$\bar{M}_2$	v_k(km/h)	$\bar{M}_1$	$\bar{M}_2$
30	72.35%	50.94%	80	70.00%	70.00%
40	71.88%	56.76%	90	69.53%	71.88%
50	71.41%	61.18%	100	69.24%	73.65%
60	70.94%	64.88%	110	68.82%	75.18%
70	70.35%	67.82%	120	68.59%	76.41%

Table 10. Comparison of $\bar{M}_1$, $\bar{M}_2$ at different v_k.

Analysis of results

Looking at the results of the three route optimization models, when considering only the damage index and the waiting time index, priority is given to delivering affected sites with higher rainfall and closer to the primary service centers; when considering only the total delivery time, the route with higher actual speed is preferred and the total distance is minimized.

And through Table 9, it can be found that the difference between the results of the three models is not very obvious. Original route optimization model shows an improvement in satisfaction over the route optimization model that only considers the damage index and the waiting time index; while the model that only requires only the shortest total time of delivery shows a small improvement over the results obtained from the route optimization model that only considers the damage index and the waiting time index.

Analysis of application scenario

The original route optimization model is more applicable to the situation where the demand supplies cannot be fully satisfied; while the route optimization model that only considers the disaster index and waiting time index is more applicable to the situation where the demand supplies can be fully satisfied; for the route optimization model that only requires the shortest total time of distribution, this means that the total distance covered by the vehicle is also reduced, which is more appropriate in scenarios where damage is light and the difference in the level of damage in the affected area is small, thus reducing the emissions and economic cost of the rescue and ensuring its effectiveness.

The effect of v_k on $\bar{M}$

The following discussion will explore the change in the average satisfaction of residents in the affected area when v_k in the distribution strategy is increased from 30 km/h to 120 km/h (each increase of 10 km/h). Assuming that the residents receive timely and effective information and can accurately ascertain v_k in the distribution strategy, the average satisfaction of the residents is $\bar{M}_1$. Conversely, if the residents are not provided with sufficient information and instead believe v_k is fixed at 80 km/h, the average satisfaction level is $\bar{M}_2$. The results are shown in Table 10; Fig. 8.

By analyzing the results of the tests, the following results were obtained.

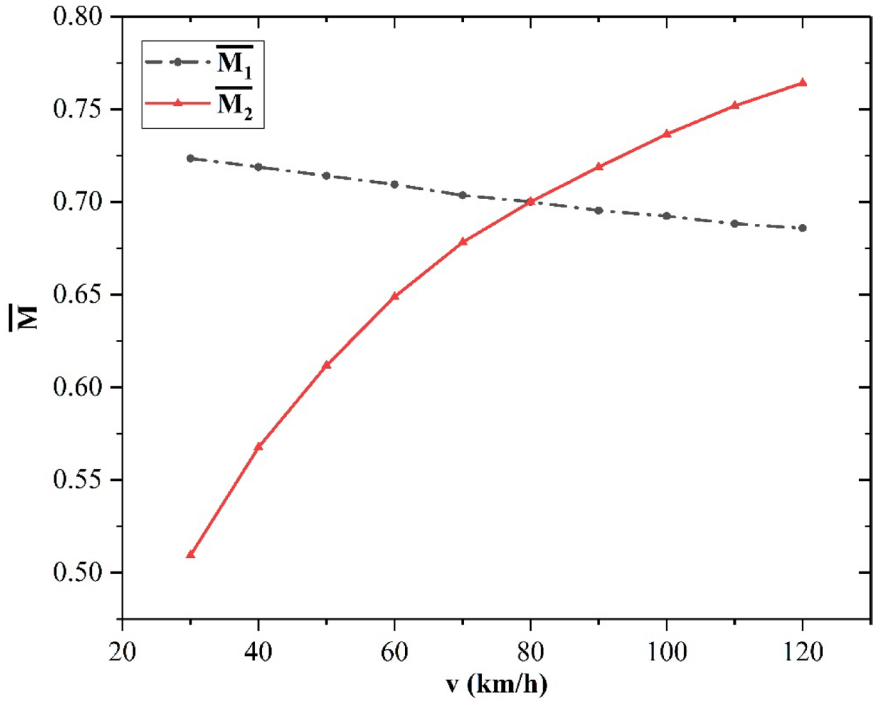

Fig. 8. Correlation of v_k with $\bar{M}_1$, $\bar{M}_2$.

The inverse relationship between $\bar{M}_1$ and v_k is attributable to the discrepancy between v'_{kij} and v_k due to precipitation. In circumstances of open and transparent information, victims will adapt their psychological expectations according to v_k with flexibility. Furthermore, an increase in v_k will not result in a significant reduction in waiting time, and the decrease in waiting time will be less than the increase in victims' psychological expectations, leading to the conclusion that as v_k increases, $\bar{M}_1$ decreases.

The positive relationship between $\bar{M}_2$ and v_k suggests that when v_k is lower than the victims' expectation, the psychological gap increases and $\bar{M}_2$ decreases. When v_k is higher than the victim's expectation, the psychological expectation is exceeded and $\bar{M}_2$ increases.

Conclusions

After a flood disaster, it is essential that emergency distribution takes place taking into account the current relief situation. The first step is to determine whether available supplies can meet the needs of all affected locations. Once this is determined, the distribution plan must be adjusted to ensure an even distribution of aid throughout the affected area.

If the severity of the disaster is evenly distributed, distribution model I can be used. Conversely, if the severity of the disaster is unevenly distributed, distribution model II can be used.

In the event that the amount of existing supplies is sufficient to cover the needs of all affected locations, the route optimization model can be used taking into account only the disaster index and the waiting time index. Conversely, if the amount of existing supplies is insufficient to meet the needs of all affected locations, the route optimization model can be used taking into account the resource scarcity index, the disaster index and the waiting time index. In cases where the situation cannot be captured, the route optimization model can be used with the aim of achieving the shortest overall distribution time. In the event that a determination is not possible, the route optimization model can be used, which only requires the shortest total distribution time.

Compared to other related studies, the approach stands out for considering the effects of precipitation on vehicle speed when deriving distribution routes. Many existing studies overlook this factor, but have found that taking this factor into account makes the routes more practical. During real floods, rainfall can significantly slow down vehicles, affecting travel times. Incorporating these variables into the model can generate more accurate distribution routes, reducing delays and ensuring timely delivery of relief supplies.

This article has several limitations. The distribution of precipitation in real situations may differ from the assumptions made in this article. The influence of topography on vehicle movement is not taken into account in the path optimization model. The influence of precipitation on vehicle speed depends on factors such as water depth, road floats, etc.

In the next phase of research, the disaster scenarios should be expanded so that the research model can be adapted to multiple types of disaster relief and the applicability of the model is improved. In addition, road network data should also be used for research closer to reality.

Data availability

All data that support the findings of this study are presented in the manuscript. Some or all mod-els or codes that support the findings of this study are available from the corresponding author upon reasonable request.

Received: 19 December 2024; Accepted: 1 July 2025
Published online: 19 August 2025

References

1. Suwanno, P. et al. Estimation of the evacuation time according to different flood depths. *Sustainability* **15**, 6305 (2023).
2. Centre for Research on the Epidemiology of Disasters. Emergency Events Database (EM-DAT). Université catholique de Louvain. (2023).
3. Maya Duque, P. A., Dolinskaya, I. S. & Sörensen, K. Network repair crew scheduling and routing for emergency relief distribution problem. *Eur. J. Oper. Res.* **248**, 272–285 (2016).
4. Baykal, T., Terzi, S. & Taylan, E. D. Examination of safe routes for emergency responders and people during urban flood: a case study of isparta, Türkiye. *Nat. Hazards*. **119**, 1379–1397 (2023).
5. Zhang, H., Huang, Y., Geng, Z. & Chen, T. Effectiveness evaluation of emergency rescuing plans oriented to urban waterlogging based on a neural network model. *IEEE Access*. **12**, 30482–30494 (2024).
6. Mitsakis, E., Stamos, I., Diakakis, M. & Salanova Grau, J. M. Impacts of high-intensity storms on urban transportation: applying traffic flow control methodologies for quantifying the effects. *Int. J. Environ. Sci. Technol.* **11**, 2145–2154 (2014).
7. Su, B., Huang, H. & Li, Y. Integrated simulation method for waterlogging and traffic congestion under urban rainstorms. *Nat. Hazards*. **81**, 23–40 (2016).
8. Pregnolato, M., Ford, A., Wilkinson, S. M. & Dawson, R. J. The impact of flooding on road transport: A depth-disruption function. *Transp. Res. Part. D: Transp. Environ.* **55**, 67–81 (2017).
9. Borowska-Stefańska, M. et al. Changes in intra-city transport accessibility accompanying the occurrence of an urban flood. *Transp. Res. Part. D: Transp. Environ.* **126**, 104040 (2024).
10. Shao, W. et al. The application of big data in the analysis of the impact of urban floods: A case study of Qianshan river basin. *J. Phys. : Conf. Ser.* **1955**, 012061 (2021).
11. Holguín-Veras, J., Pérez, N., Jaller, M., Van Wassenhove, L. N. & Aros-Vera, F. On the appropriate objective function for post-disaster humanitarian logistics models. *J. Oper. Manag.* **31**, 262–280 (2013).
12. Shi, W., He, J., Wang, M. & Yang, F. A dynamics model of the emergency medical supply chain in epidemic considering deprivation cost. *Socio-Economic Plann. Sci.* **94**, 101924 (2024).
13. Chen, M., Zhou, S., Gong, Y. & Tang, L. Medical emergency supplies dispatching vehicle path optimization based on demand urgency. *Applied Math. Nonlinear Sciences* **9**, 00270 (2023).
14. Liu, J., Bai, J. & Wu, D. Medical supplies scheduling in major public health emergencies. *Transp. Res. E.* **154**, 102464 (2021).
15. Khalili-Fard, A. et al. Integrated relief pre-positioning and procurement planning considering non-governmental organizations support and perishable relief items in a humanitarian supply chain network. *Omega* **127**, 103111 (2024).
16. Ghasemi, P., Goodarzian, F. & Abraham, A. A new humanitarian relief logistic network for multi-objective optimization under stochastic programming. *Appl. Intell.* **52**, 13729–13762 (2022).
17. Zokaee, S., Bozorgi-Amiri, A. & Sadjadi, S. J. A robust optimization model for humanitarian relief chain design under uncertainty. *Appl. Math. Model.* **40**, 7996–8016 (2016).
18. Yang, H., Zhang, P., Zhang, P., Zhang, C. & Yan, X. Optimization of a two-stage emergency logistics system considering public psychological risk perception under earthquake disaster. *Sci. Rep.* **14**, 31983 (2024).
19. Valero, D., Bayón, A. & Franca, M. J. Urban flood drifters (UFDs): onset of movement. *Sci. Total Environ.* **927**, 171568 (2024).
20. Zang, Y., Huang, J. & Wang, H. Dynamic impact assessment of urban floods on the compound Spatial network of buildings-roads-emergency service facilities. *Sci. Total Environ.* **926**, 172007 (2024).
21. Okonta, S. D. & Olaomi, J. Applying network flow optimisation techniques to minimise cost associated with flood disaster. *Jàmbá: J. Disaster Risk Stud.* **15**, 1–13 (2023).
22. Zhu, L., Gong, Y., Xu, Y. & Gu, J. Emergency relief routing models for injured victims considering equity and priority. *Ann. Oper. Res.* **283**, 1573–1606 (2019).
23. Lam, W. H. K., Tam, M. L., Cao, X. & Li, X. Modeling the effects of rainfall intensity on traffic speed, flow, and density relationships for urban roads. *J. Transp. Eng.* **139**, 758–770 (2013).
24. Gong, D., Song, G., Li, M., Gao, Y. & Yu, L. Impact of rainfalls on travel speed on urban roads. *J. Transp. Syst. Eng. Inf. Technol.* **15**, 218–225 (2015). (in Chinese).
25. Holguín-Veras, J. et al. Econometric Estimation of deprivation cost functions: A contingent valuation experiment. *J. Ops Manage.* **45**, 44–56 (2016).
26. Dantzig, G. B. & Ramser, J. H. The truck dispatching problem. *Manage. Sci.* **6**, 80–91 (1959).
27. Kumar, B. A. et al. Hybrid genetic algorithm-simulated annealing based electric vehicle charging station placement for optimizing distribution network resilience. *Sci. Rep.* **14**, 7637 (2024).

Author contributions

Conceptualization, Pei. Z and C. Z; Methodology, Pei. Z and C. Z; Writing-Reviewing and Editing, Pei. Z; Software, C. Z; Writing- Original draft preparation, C. Z; Supervision, H. Y and X. Y; Visualization, H. Y; Investigation, H. Y and Pan. Z; Validation, H. Y; Data curation, H. Y. All authors have read and agreed to the published version of the manuscript.

Funding

This work was supported by Shanxi Science and Technology Strategic Research Special Project (Grant No. 202204031401079). The financial contributions are gratefully acknowledged.

Declarations

Competing interests
The authors declare no competing interests.

Additional information
Correspondence and requests for materials should be addressed to X.Y. or H.Y.

Reprints and permissions information is available at www.nature.com/reprints.

Publisher's note Springer Nature remains neutral with regard to jurisdictional claims in published maps and institutional affiliations.